J. Plasma Physics (2004), *vol.* 70, *part* 3, *pp.* 369–378.
DOI: 10.1017/S0022377803002757 Printed in the United Kingdom

Electron temperature gradient driven electromagnetic-drift wave instability and associated electron thermal diffusion in a magnetized plasma

A. A. MAMUN† and P. K. SHUKLA

Institut für Theoretische Physik IV, Fakultät für Physik und Astronomie,
Ruhr-Universität Bochum, D-44780 Bochum, Germany
(ps@tp4.ruhr-uni-bochum.de)

(Received 21 August 2003, in revised form 13 October 2003 and accepted 14 October 2003)

Abstract. The electron temperature gradient driven electromagnetic-drift waves and associated instabilities and electron thermal diffusion in a magnetized plasma have been investigated by employing kinetic ion and fluid electron responses. A new dispersion relation has been derived analytically and studied numerically. Two broad classes of unstable fluctuations, namely 'low' and 'high' frequency unstable modes, have been identified and studied in detail. The instabilities of these modes and associated electron thermal diffusion coefficients are also estimated. The results of our theoretical model can be considered as a plausible explanation for experimentally observed fluctuations in Burke et al. (2000a *Phys. Plasmas* **7**, 1397).

1. Introduction

It is well known (Mikhailovskii 1992, 1998) that magnetized laboratory and space plasmas contain free energy sources in the form of equilibrium pressure and magnetic field gradients. The latter can cause different classes of micro-instabilities involving electrostatic drift and electromagnetic drift–Alfvén waves (Mikhailovskii 1992). Non-thermal fluctuations can produce anomalous cross-field charged particle and heat transport (Kadomtsev 1965, Horton et al. 1965), which degrade the plasma confinement. Accordingly, a complete knowledge of waves and instabilities in a non-uniform magnetoplasma is very essential for understanding the instability and transport processes in laboratory and space plasmas.

Recently, Burke et al. (2000a, b) and Maggs and Morales (2003) have performed several laboratory experiments to demonstrate the spatio-temporal properties of spontaneous fluctuations that are triggered by gradients in the ambient plasma parameters, namely density, temperature, magnetic field, etc. They observed two kinds of broadband fluctuations. One is identified (Burke et al. 2000a) as a low-frequency ($\omega \sim 0.02\ \omega_{ci}$) temperature fluctuation mode and the other as a relative high-frequency ($\omega \sim 0.1\ \omega_{ci}$) drift–Alfvén mode, where ω (ω_{ci}) is the mode frequency (ion gyrofrequency). In this paper, we present a theoretical explanation for

† Permanent address: Department of Physics, Jahangirnagar University, Savar, Dhaka, Bangladesh.

those experimental observations. Specifically, we theoretically investigate the electron temperature gradient driven electromagnetic-drift waves and associated non-thermal transport coefficients (namely the electron thermal diffusion coefficient) in a magnetized plasma by employing a kinetic description for ions and a fluid description for electrons. We identify two broad classes of unstable fluctuations, namely low- and high-frequency unstable modes, and study their existence regimes in detail. The results of our theoretical model can be considered as a plausible explanation for experimentally observed fluctuations in Burke et al. (2000a).

The manuscript is organized as follows. The electron and ion number density perturbations are obtained by using a kinetic (fluid) description for ions (electrons) in Sec. 2. The general dispersion relation for the electron temperature gradient driven electromagnetic-drift waves is derived and investigated both analytically and numerically in Sec. 3. The electron thermal diffusion coefficient associated with unstable low- and high-frequency waves are estimated in Sec. 4. Finally, a brief discussion is given in Sec. 5.

2. Electron and ion responses

We consider a fully ionized, two-component (electron–ion), collisionless plasma with an equilibrium electron temperature gradient. We assume that the plasma is embedded in a homogeneous magnetic field $\hat{\mathbf{z}}B_0$, where $\hat{\mathbf{z}}$ is the unit vector along the z-direction, and that the equilibrium electron temperature gradient is in a direction perpendicular to the direction of the external magnetic field (namely along the x-direction). We are interested in examining the obliquely propagating low-frequency electromagnetic waves with the frequency satisfying $\omega \ll \omega_{ce}$ (where $\omega_{ce} = eB_0/m_e c$ is the electron gyrofrequency, e is the magnitude of the electron charge, m_e is the electron mass, and c is the speed of light in vacuum) in such a magnetoplasma. Thus, in the presence of low-frequency electromagnetic fields, $\mathbf{E} = -\nabla\phi - \hat{\mathbf{z}}c^{-1}\partial_t A_z$ and $\mathbf{B} = \nabla A_z \times \hat{\mathbf{z}}$, where ϕ is the scalar potential, A_z is the z-component of the vector potential and $\partial_t = \partial/\partial t$, we can express the perpendicular and parallel components of the electron fluid velocities ($\mathbf{u}_{e\perp}$ and u_{ez}) as

$$\mathbf{u}_{e\perp} \simeq \frac{c}{B_0}\left[\hat{z}\times\nabla\phi - \frac{1}{en_e}\hat{z}\times\nabla(n_e T_e)\right], \tag{2.1}$$

$$u_{ez} \simeq \frac{c}{4\pi e n_e}\nabla_\perp^2 A_z \tag{2.2}$$

where n_e is the electron number density and T_e is the electron temperature in units of the Boltzmann constant. To derive (2.2), we have used Ampere's law along with an assumption that the current parallel to $\hat{\mathbf{z}}$ is mainly carried by the electrons.

Now, using (2.1) and (2.2) we can express the electron continuity equation, the z-component of the electron equation of motion and the electron energy equation in linearized form as

$$\partial_t n_{e1} + \frac{c}{4\pi e}\nabla_\perp^2 \partial_z A_z = 0, \tag{2.3}$$

$$(\partial_t + V_\star \partial_y)A_z + c\partial_z\left(\phi - \frac{T_{e0}}{e}\frac{n_{e1}}{n_0} - \frac{T_{e1}}{e}\right) = 0, \tag{2.4}$$

$$\left(\partial_t - \frac{2}{3}\Omega_T\right)T_{e1} + eV_\star\partial_y\phi = \frac{2T_{e0}}{3n_0}\left(\partial_t - \Omega_n\right)n_{e1}, \tag{2.5}$$

https://doi.org/10.1017/S0022377803002757 Published online by Cambridge University Press

where $\partial_y = \partial/\partial y$, $V_\star = k_T V_{Te}^2/\omega_{ce}$, $V_{Te} = (T_{e0}/m_e)^{1/2}$, $k_T = -T_{e0}^{-1}\partial_x T_{e0}$, $\Omega_T = -n_0^{-1}(\partial\mathscr{L}/\partial T_e)_{T_{e0}}$, $\Omega_n = T_{e0}^{-1}(\partial\mathscr{L}/\partial n_e)_{n_0}$, and $\mathscr{L}$ is a generalized heat loss function (a function of n_e and T_e), and is defined as energy losses minus energy gains, per unit of volume per unit of time. n_{e1} (T_{e1}) is the perturbed part of the electron number density (temperature), n_0 (T_{e0}) is the equilibrium part of the electron number density (temperature). Using (2.3) and (2.5) in (2.4) we obtain a single equation relating n_{e1} and ϕ in the form

$$\left[\left(\hat{O}\partial_t + V_A^2\rho_s^2\nabla_\perp^2\partial_z^2\right)\hat{P} + \frac{2}{3}V_A^2\rho_s^2\nabla_\perp^2\partial_z^2\hat{Q}\right] n_{e1} = \frac{c^2}{4\pi e}\nabla_\perp^2\partial_z^2\left(\hat{O} - \frac{2}{3}\Omega_T\right)\phi, \qquad (2.6)$$

where $\hat{O} = \partial_t + V_\star\partial_y$, $\hat{P} = \partial_t - 2\Omega_T/3$, $\hat{Q} = \partial_t - \Omega_n$, $V_A = (B_0^2/4\pi n_0 m_i)^{1/2}$, $\rho_s = c_s/\omega_{ci}$, and $c_s = (T_{e0}/m_i)^{1/2}$. We now assume that n_{e1} and ϕ are proportional to $\exp(-i\omega t + ik_y y + ik_z z)$, where k_y (k_z) are y (z) components of the wave propagation vector $\mathbf{k}$, i.e. $k_y = k\sin\theta$ and $k_z = k\cos\theta$ with $\theta = \tan^{-1}(k_y/k_z)$ being the angle between the directions of $\mathbf{B}_0$ and $\mathbf{k}$. Hence, (2.6) can be Fourier transformed to obtain

$$n_{e1} = -\frac{k_y^2}{4\pi e}\frac{k_z^2c^2\left(\Omega_\star - i\frac{2}{3}\Omega_T\right)\phi}{\left(\Omega_\star\omega - \Omega_A^2\right)\left(\omega - i\frac{2}{3}\Omega_T\right) - \frac{2}{3}\Omega_A^2(\omega - i\Omega_n)}, \qquad (2.7)$$

where $\Omega_\star = \omega - k_y V_\star$ and $\Omega_A = k_z V_A k_y \rho_s$. We next present the expression for the ion number density perturbation n_{i1} which can be deduced from the Vlasov equation (Brambilla 1998; Rao and Kaup 1992; Shukla and Stenflo 2000). Thus, we have

$$n_{i1} \simeq -\frac{n_0 e}{T_i}\left[1 - \Gamma_0(b_i) - \frac{2\Gamma_1(b_i)\omega^2}{\omega^2 - \omega_{ci}^2}\right]\phi, \qquad (2.8)$$

where T_i is the ion temperature in units of the Boltzmann constant, $\Gamma_{0,1} = I_{0,1}\exp(-b_i)$, I_0 (I_1) is the zero (first) order modified Bessel function with argument $b_i = k_y^2\rho_i^2$, $\rho_i = V_{Ti}/\omega_{ci}$ is the ion Larmor radius, $V_{Ti} = (T_i/m_i)^{1/2}$ is the ion thermal speed, $\omega_{ci} = eB_0/m_i c$ is the ion gyrofrequency, and m_i is the ion mass. We note that for $b_i \ll 1$, (2.8) reduces to $n_{i1} \simeq k_y^2 n_0 e\phi/[m_i(\omega^2 - \omega_{ci}^2)]$, which for $\omega \ll \omega_{ci}$ can be further simplified as $n_{i1} \simeq -(c^2k_y^2n_0m_i/eB_0^2)\phi$. On the other hand, for $b_i \gg 1$, (2.8) reduces to $n_{i1} \simeq -(n_0e/T_i)\phi$.

3. Dispersion properties

By invoking the quasineutrality condition $n_{e1} = n_{i1}$ as well as (2.7) and (2.8), we obtain the general dispersion relation

$$1 - \Gamma_0(b_i) - 2\Gamma_1(b_i)\frac{\omega^2}{\omega^2 - \omega_{ci}^2} = \frac{k_z^2V_A^2k_y^2\rho_i^2\left(\Omega_\star - i\frac{2}{3}\Omega_T\right)}{\left(\Omega_\star\omega - \Omega_A^2\right)\left(\omega - i\frac{2}{3}\Omega_T\right) - \frac{2}{3}\Omega_A^2(\omega - i\Omega_n)}. \qquad (3.1)$$

Our new dispersion relation given by (3.1) does not impose any restriction on the values of ω/ω_{ci} and b_i. Before going to the numerical analysis of (3.1), let us briefly discuss the following two limiting cases.

3.1. Ion fluid limit

When we neglect the ion Larmor radius effect, i.e. $b_i \ll 1$, the dispersion relation for the low-frequency electromagnetic waves satisfying $\omega/\omega_{ci} \ll 1$ can be simplified as

$$\omega^3 - \Omega_{T\star}\omega^2 - \left(\alpha k_z^2V_A^2 - i\tfrac{2}{3}\Omega_T\omega_\star\right)\omega + \left(\omega_\star + i\tfrac{2}{3}\Omega_{L1}\right)k_z^2V_A^2 = 0, \qquad (3.2)$$

https://doi.org/10.1017/S0022377803002757 Published online by Cambridge University Press

where $\alpha = 1 + 5k_y^2\rho_s^2/3$, $\omega_\star = k_y V_\star$, $\Omega_{T\star} = \omega_\star + i2\Omega_T/3$, $\Omega_{L1} = \Omega_T + \Omega_L k_y^2\rho_s^2$, and $\Omega_L = \Omega_T + \Omega_n$. For parallel propagation ($k_y = 0$), (3.2) reduces to $(\omega - k_z V_A)(\omega - 2i\Omega_T/3) = 0$ which represents two uncoupled modes, namely the shear Alfvén waves $\omega = k_z V_A$ and a purely growing radiative thermal mode $\omega = i2\Omega_T/3$. On the other hand, for perpendicular propagation ($k_z = 0$), from (3.2) we have $(\omega - k_y V_\star)(\omega - 2i\Omega_T/3) = 0$, which represents two uncoupled modes, namely the electron temperature gradient driven drift waves $\omega = k_y V_\star$, and a purely growing radiative thermal mode $\omega = i2\Omega_T/3$.

For oblique propagation (3.2) represents the dispersion relation for the coupled drift–Alfvén waves modified by the electron inertia, fluctuation of the electron temperature and radiative energy loss. To examine the instability of the coupled drift–Alfvén waves, we have to numerically solve (3.2). However, for $\omega \sim k_y V_\star \ll k_z V_A$ (3.2) can be approximated as

$$\omega \simeq \frac{k_y V_\star}{1 + \frac{5}{3}k_y^2\rho_s^2} + i\frac{2\left(\Omega_T + \Omega_L k_y^2\rho_s^2\right)}{3\left(1 + \frac{5}{3}k_y^2\rho_s^2\right)}. \tag{3.3}$$

Equation (3.3) represents unstable electron temperature gradient driven drift waves with the real frequency $\omega_k \simeq k_y V_\star/(1 + 5k_y^2\rho_s^2/3)$ and the growth rate $\gamma_k \simeq 2(\Omega_T + \Omega_L k_y^2\rho_s^2)/3(1 + 5k_y^2\rho_s^2/3)$.

3.2. Strong ion Larmor radius effect

When we consider an extremely strong Larmor radius effect, i.e. for $b_i \gg 1$, the dispersion relation (3.1) can be simplified as

$$\omega^3 - \Omega_{T\star}\omega^2 - \left(\sigma k_z^2 V_A^2 - i\tfrac{2}{3}\Omega_T\omega_\star\right)\omega + \left(\omega_\star + i\tfrac{2}{3}\Omega_{L2}\right)b_i k_z^2 V_A^2 = 0, \tag{3.4}$$

where $\sigma = (1 + 5T_{e0}/3T_i)b_i$ and $\Omega_{L2} = \Omega_T + T_{e0}\Omega_L/T_i$. Since $k_y^2\rho_i^2 \gg 1$ is assumed, in (3.4) we cannot consider the parallel propagation. However, for perpendicular propagation ($k_z = 0$), from (3.4) we obtain the two uncoupled modes (namely the electron temperature gradient driven drift waves $\omega = k_y V_\star$, and a purely growing radiative thermal mode $\omega = i2\Omega_T/3$) that we obtained in the fluid limit ($b_i \ll 1$). Now, for oblique propagation and for $\omega \sim k_y V_\star \ll b_i k_z V_A$, (3.4) can be approximated as

$$\omega \simeq \frac{k_y V_\star}{1 + 5T_{e0}/3T_i} + i\frac{2(\Omega_T + (T_{e0}/T_i)\Omega_L)}{3(1 + 5T_{e0}/3T_i)}. \tag{3.5}$$

Equation (3.5) represents the unstable electron temperature gradient driven drift waves with the real frequency $\omega_k = k_y V_\star/(1 + 5T_{e0}/3T_i)$ and the growth rate $\gamma_k \simeq 2(\Omega_T + T_{e0}\Omega_L/T_i)/3(1 + 5T_{e0}/3T_i)$ including the effect of the strong ion Larmor radius effect.

3.3. Numerical analysis

The waves and associated instabilities that we have discussed are restricted to two limiting cases, namely $b_i \ll 1$ and $b_i \gg 1$. The former is further restricted to $\omega \ll \omega_{ci}$. To have more general results (without imposing any restriction on the values of ω/ω_{ci} and b_i), we now numerically solve (3.1) and find its real and imaginary solutions for typical laboratory plasma parameters (Burke et al. 2000a; Maggs and Morales 2003): $T_{e0} \simeq 5$ eV, $B_0 \simeq 1$ kG, $n_0 \simeq 10^{12}$ cm^{-3}, $T_i \simeq 0.2T_{e0}$, and $\Omega_n/\omega_{ci} \simeq 0.1$. The numerical results are displayed in Figs. 1–5. We have found in our numerical analysis that for the above-mentioned typical laboratory plasma parameters, the

https://doi.org/10.1017/S0022377803002757 Published online by Cambridge University Press

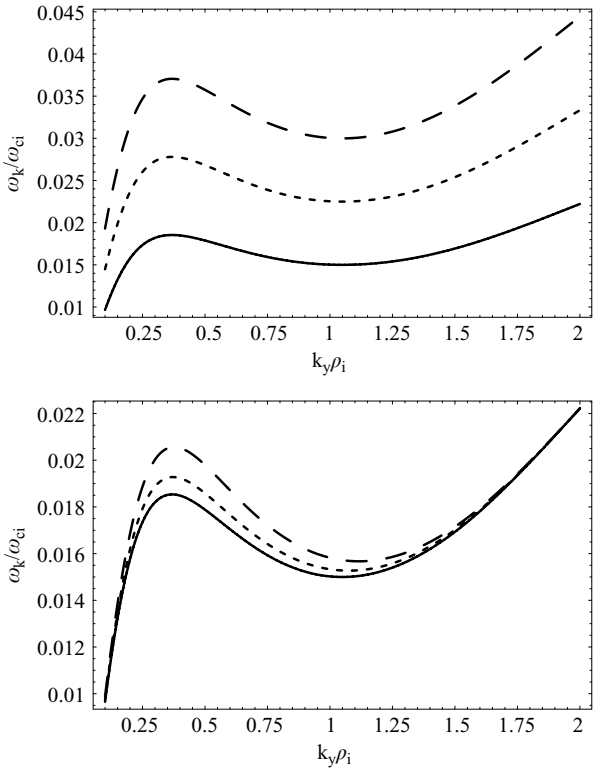

Figure 1. The dispersion properties of the low-frequency mode for typical plasma parameters given in the text. The upper plot represents the dispersion properties for $\Omega_T/\omega_{ci} = 0.2$, $k_T = 2$ cm^{-1} (solid curve), 3 cm^{-1} (dotted curve), and 4 cm^{-1} (dashed curve). The lower plot represents the dispersion properties for $k_T = 2$ cm^{-1}, $\Omega_T/\omega_{ci} = 0.2$ (solid curve), 0.5 (dotted curve), and 0.8 (dashed curve). Here the frequency ω_k is found to be independent of θ.

dispersion relation (3.1) has two positive real roots and three positive imaginary roots. The two positive real roots represent two eigenmodes: one is a low-frequency mode and other is a high-frequency mode. The dispersion properties of low-frequency mode are shown in Fig. 1 and those of the high-frequency mode are shown in Fig. 2.

Figure 1 shows how the frequency ω_k of the low-frequency mode varies with $k_y\rho_i$ for different values of k_T (cf. the upper plot of Fig. 1) and Ω_T (cf. the lower plot of Fig. 1). The real solutions corresponding to the low-frequency mode were found to be independent of θ. Figure 2 shows how the frequency ω_k of the high-frequency mode varies with $k_y\rho_i$. The upper (lower) plot of Fig. 2 shows how the dispersion properties of this high-frequency mode for a long (short) wavelength perpendicular to the magnetic field varies with θ (k_T). The frequency ω_k is found to be independent of k_T and Ω_T for a long perpendicular wavelength limit ($k_y\rho_i \leq 0.1$) and independent of θ and Ω_T for a short perpendicular wavelength limit ($k_y\rho_i > 0.1$). Figure 3 shows how the growth rate γ_k of the unstable low-frequency mode varies with $k_y\rho_i$ for different values of k_T (cf. the upper plot of Fig. 3) and Ω_T (cf. the lower plot of Fig. 3). The imaginary solutions corresponding to the low-frequency mode are found to be independent of θ. Figure 4 shows how the growth rate γ_k of a

https://doi.org/10.1017/S0022377803002757 Published online by Cambridge University Press

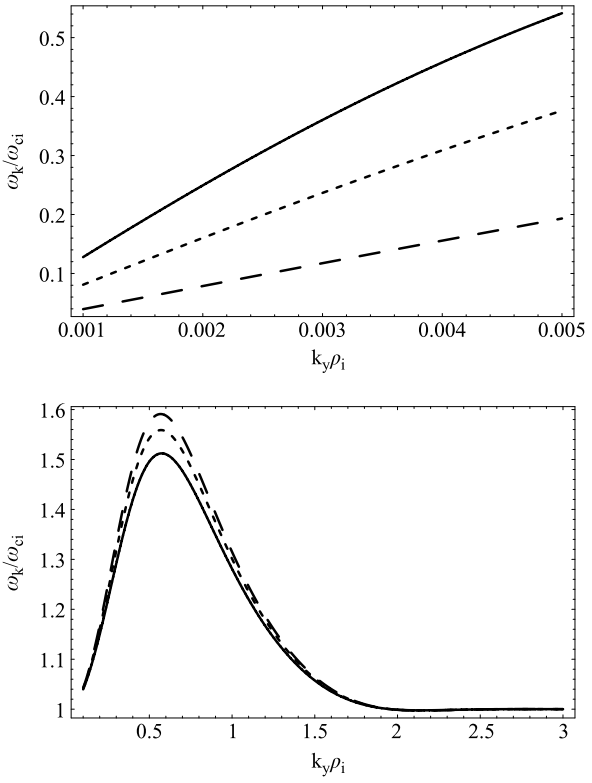

Figure 2. The dispersion properties of the high-frequency mode for the typical plasma parameters given in the text. The upper plot represents the dispersion properties of the waves corresponding to long-wavelength perpendicular to the magnetic field for $\theta = 60°$ (solid curve), 70° (dotted curve) and 80° (dashed curve). The lower plot represents the dispersion properties of the waves corresponding to short-wavelength perpendicular to the magnetic field for $k_T = 2$ cm^{-1} (solid curve), 10 cm^{-1} (dotted curve) and 15 cm^{-1} (dashed curve). The frequency ω_k corresponding to the long-wavelength limit (cf. the upper plot) was found to be independent of Ω_T and k_T. The frequency ω_k corresponding to the short-wavelength limit (cf. the lower plot) was found to be independent of θ and Ω_T.

purely growing radiative thermal mode varies with $k_y\rho_i$ for different values of k_T. The growth rate γ_k of this purely growing radiative thermal mode is found to be independent of k_T and θ. Figure 5 shows how the growth rate γ_k of the unstable high-frequency mode varies with $k_y\rho_i$ for different values of k_T (cf. the upper plot of Fig. 5) and Ω_T (cf. the lower plot of Fig. 5). The imaginary solutions corresponding to the high-frequency mode are found to be independent of θ.

4. Diffusion coefficient

We now estimate the diffusion coefficients D associated with low- and high-frequency modes which produce a cross-field electron thermal energy flux

$$\Gamma_x = \langle T_{e1} u_{ex} \rangle + \text{complex conjugate}, \tag{4.1}$$

where the angular brackets denote the ensemble average. For $\omega_k \ll \omega_{ce}, kc$, we can

https://doi.org/10.1017/S0022377803002757 Published online by Cambridge University Press

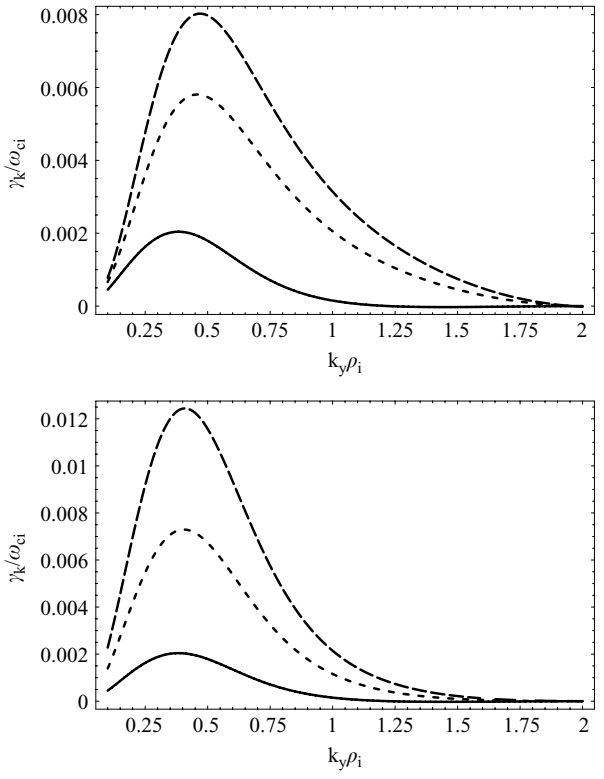

Figure 3. The growth rate γ_k of the low-frequency mode for the typical plasma parameters given in the text. The upper plot, where $\Omega_T/\omega_{ci} = 0.2$, $k_T = 2$ cm^{-1} (solid curve), 6 cm^{-1} (dotted curve) and 10 cm^{-1} (dashed curve), shows how the growth rate γ_k varies with k_T. The lower plot, where $k_T = 2$ cm^{-1}, $\Omega_T/\omega_{ci} = 0.2$ (solid curve), 0.3 (dotted curve) and 0.4 (dashed curve) shows how the growth rate γ_k varies with Ω_T. The growth rate γ_k of the low-frequency mode in both cases is found to be independent of θ.

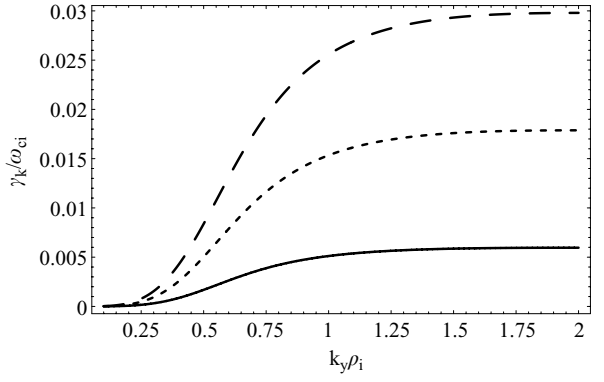

Figure 4. The growth rate γ_k of the purely growing radiative thermal mode for the typical plasma parameters given in the text, and for $\Omega_T/\omega_{ci} = 0.2$ (solid curve), 0.3 (dotted curve) and 0.4 (dashed curve). Here γ_k is found to be independent of k_T and θ.

https://doi.org/10.1017/S0022377803002757 Published online by Cambridge University Press

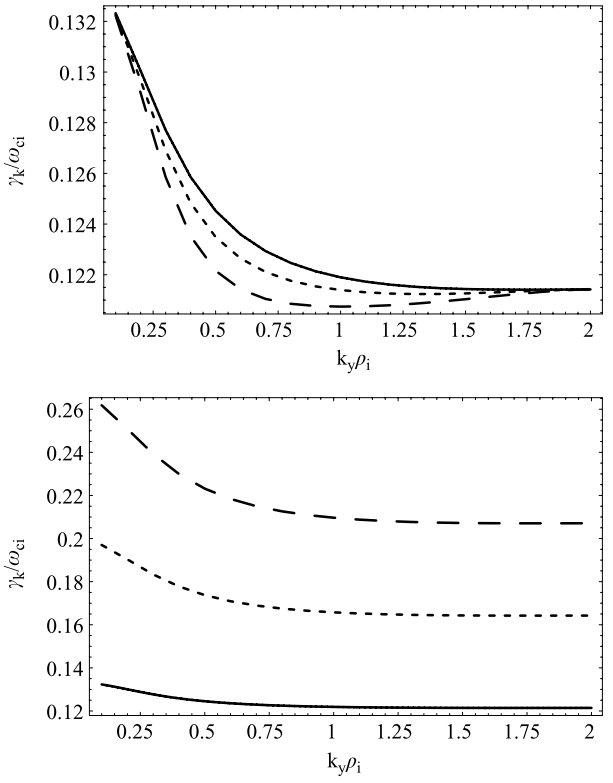

Figure 5. The growth rate γ_k of the high-frequency mode for the typical plasma parameters given in the text. The upper plot, where $\Omega_T/\omega_{ci} = 0.2$, $k_T = 2$ cm^{-1} (solid curve), 10 cm^{-1} (dotted curve) and 15 cm^{-1} (dashed curve), shows how the growth rate γ_k varies with k_T. The lower plot, where $k_T = 2$ cm^{-1}, $\Omega_T/\omega_{ci} = 0.2$ (solid curve), 0.3 (dotted curve) and 0.4 (dashed curve) shows how the growth rate γ_k varies with Ω_T. The growth rate γ_k of the low-frequency mode in both cases is found to be independent of θ.

express u_{ex} and T_{e1} as

$$u_{ex} = -i\frac{ck_y}{B_0}\phi_k, \tag{4.2}$$

$$T_{e1} = \left(\frac{k_y V_\star}{\omega_k} - \frac{2}{3}k_y^2\rho_s^2 - i\frac{k_y V_\star \gamma_k}{\omega_k^2}\right)e\phi_k, \tag{4.3}$$

where ω_k and γ_k are the real and imaginary parts of the wave frequency ω corresponding to a fixed k. Now, using (4.1)–(4.3) and Fick's law $\Gamma_x = -D\partial_x T_{e0}$, the diffusion coefficient corresponding to a fixed k can be approximated as

$$D_k \approx \pi^2\frac{\gamma_k}{k^2}. \tag{4.4}$$

We note that in order to derive (4.4) we used $\langle\phi_k\rangle \simeq \pi B_0\omega_k/ckk_y$, which is obtained by using the mixing length hypothesis. Taking $k_y\rho_i \simeq 1$, $\theta = 60^\circ$ and the corresponding $\gamma_k/\omega_{ci} \simeq 0.003$ from the dashed curve in the upper plot of Fig. 3, we estimate the diffusion coefficient (associated with the low-frequency waves) $D_k \simeq \pi^2 0.003\ \omega_{ci}\rho_i^2 \sin^2\theta \approx 1.5\times10^3$ cm^2 s^{-1}. On the other hand, taking $k_y\rho_i \simeq 1$

https://doi.org/10.1017/S0022377803002757 Published online by Cambridge University Press

and the corresponding $\gamma_k/\omega_{ci} \simeq 0.1215$ from the dotted curve in the upper plot of Fig. 5, we can estimate the diffusion coefficient (associated with the high-frequency waves) $D_k \simeq \pi^2 0.1215\, \omega_{ci}\rho_i^2 \sin^2\theta \approx 6 \times 10^4$ cm^2 s^{-1}. We note that in our numerical analysis (Figs. 1–5), we used $k_z = k_y \cot\theta$ which means that k_z and $k = \sqrt{k_y^2 + k_z^2}$ vary with k_y for fixed θ.

5. Discussion

We have investigated the electron temperature gradient driven electromagnetic-drift waves and associated instabilities and transport coefficients (namely the electron thermal diffusion coefficient) in a magnetized plasma by employing a kinetic description for ions and a fluid description for electrons. We have derived a new dispersion relation, which has been investigated first analytically in two limits (namely $k_y\rho_i \ll 1$ and $k_y\rho_i \gg 1$) and then numerically in general. We have found two broad classes of unstable fluctuations: one is a low-frequency temperature fluctuation mode with the frequency $\omega_k \sim 0.02\ \omega_{ci}$ (cf. Fig. 1) and the other is a relative high-frequency drift–Alfvén mode with the frequency $\omega_k \sim 0.1\ \omega_{ci}$ (cf. the upper plot of Fig. 2). We have also studied the dispersion properties of these modes and associated instabilities in detail. The growth rates of these modes are found to be a fraction of the frequency of the corresponding mode (cf. Figs. 3 and 5).

We have found in our numerical analysis that for the typical laboratory plasma parameters (Burke et al. 2000a; Maggs and Morales 2003) the dispersion relation (3.1) has two positive real roots and three positive imaginary roots. The two positive real roots represent two eigenmodes: one is a low-frequency mode (cf. Fig. 1) and other is a high-frequency mode (cf. Fig. 2). The three positive imaginary roots represent the growth rates of the low-frequency mode (cf. Fig. 3), the purely growing radiative thermal mode (cf. Fig. 4) and the high-frequency mode (cf. Fig. 5), respectively. We have also estimated the electron thermal diffusion coefficient associated with the unstable low- and high-frequency modes for typical laboratory plasma parameters (Burke et al. 2000a; Maggs and Morales 2003): $T_{e0} \simeq 5$ eV, $B_0 \simeq 1$ kG, $n_0 \simeq 10^{12}$ cm^{-3}, $T_i \simeq 0.2T_{e0}$, $\Omega_n/\omega_{ci} \simeq 0.1$, $\Omega_T/\omega_{ci} = 0.2$, $k_T = 10$ cm^{-1} and $k_y\rho_i \simeq 1$. The electron diffusion coefficient D_k turns out to be $\sim 1.5 \times 10^3$ cm^2 s^{-1} and $\sim 6 \times 10^4$ cm^2 s^{-1} for the low- and high-frequency modes, respectively. The results of our theoretical model can be considered as a plausible explanation for experimentally observed fluctuations in Burke et al. (2000a).

Acknowledgement

A. A. Mamun gratefully acknowledges the financial support of the Alexander von Humboldt-Stiftung (Bonn, Germany).

References

Brambilla, M. 1998 *Kinetic Theory of Plasma Waves: Homogeneous Plasmas*. Oxford: Clarendon Press, p. 333.

Burke, A. T., Maggs, J. E. and Morales, G. J. 2000a *Phys. Plasmas* **7**, 1397.

Burke, A. T., Maggs, J. E. and Morales, G. J. 2000b *Phys. Rev. Lett.* **84**, 1451.

Horton, W., Hu, B. and Zhu, P. 2003 *New J. Phys.* **5**, 14.1.

Kadomtsev, B. B. 1965 *Plasma Turbulence*. London: Academic Press.

Maggs, J. E. and Morales, G. J. 2003 *Phys. Plasmas* **10**, 2267.

Mikhailovskii, A. B. 1992 *Electromagnetic Instabilities in an Inhomogeneous Plasma*. Bristol: Institute of Physics.

Mikhailovskii, A. B. 1998 *Instabilities in a Confined Plasma*. Bristol: Institute of Physics Publishing Ltd.

Rao, N. N. and Kaup, D. J. 1992 *J. Geophys Res.* **97**, 6323.

Shukla, P. K. and Stenflo, L. 2000 *J. Plasma Phys.* **64**, 125.